Mathematical model of a smoldering log

Fernando de Souza Costa [a,*], David Sandberg [b]

[a] *Laboratório Associado de Combustão e Propulsão, INPE Caixa Postal 01, Cachoeira Paulista, 12630-000, Brazil*
[b] *Forestry Sciences Laboratory, PNRS/USDA, Corvallis, OR, USA*

Abstract

A mathematical model is developed describing the natural smoldering of logs. It is considered the steady one-dimensional propagation of infinitesimally thin fronts of drying, pyrolysis, and char oxidation in a horizontal semi-infinite log. Expressions for the burn rates, distribution profiles of temperature, and positions of the drying, pyrolysis, and smoldering fronts are obtained in terms of the smolder temperatures. An appropriate smolder transfer number is defined. Heat transfer by conduction, convection, and radiation inside the porous matrix of the log is considered, as are convection and radiation around the log and inside the boundary layer adjacent to the smoldering end. Solutions for the problem without circumferential heat losses and for a single front of drying and pyrolysis are also presented. The effects of variations of several parameters, such as moisture content, log diameter, pyrolysis temperature, heat of char oxidation, heat of pyrolysis, porosity, fuel density, and char density, are evaluated. The theoretical burning rates are in good agreement with available experimental data.
© 2004 The Combustion Institute. Published by Elsevier Inc. All rights reserved.

Keywords: Smoldering; log; Mathematical model; Wood, char

1. Introduction

Smoldering is a flameless burning process that can occur in charring fuels, such as wood, cigarettes, and expanded polymers. The combustion reaction is heterogeneous and occurs in the interior or on the surface of the porous fuel. There has been a growing interest in the smoldering of logs after forest fires, because of environmental concerns. Smoldering logs can be a significant source of air pollutants and biomass consumption and may also initiate new fires. Most of the biomass burned in forest fires or prescribed burns is contained in large logs, which can often sustain smolder for several days after flaming. Logs can smolder during and after a fire in different geometries and may present transition to flaming or extinction. However, many trunks can show an approximately one-dimensional steady smoldering process, with most of the ash produced being deposited on soil or carried away by the wind. A substantial amount of smoke and toxic gases can be released from biomass burning. The burning products are hazardous to firefighters and local residents, and can be globally significant as greenhouse gases [1,2].

Previous work on similar smoldering problems includes modeling of smoldering cellulose cylinders [3,4], polymer cylinders [5], cigarettes [6–11], pyrolysis of wood slabs [12–14], and forced forward smoldering of porous solids and polymers [15–18]. In

* Corresponding author. Fax: +5512-3101-1992.
E-mail address: fernando@lcp.inpe.br (F. de Souza Costa).

Nomenclature

A_c	adjustment factor
B_s	smoldering transfer number
$c_{p,i}$	specific heat of substance i = f, d, c, a, w, v
$c_{p,1}$	specific heat of liquid water within the wood
$\bar{c}_{p,i}$	average specific heat of zone i = f, d, c
$d_{p,i}$	average pore diameter in zone i
h_i^*	heat convection coefficient around zone i = f, d, c
h_s	convection heat transfer coefficient at smoldering front
h_0	convection heat transfer coefficient without blowing
$h_{i,conv}$	convective heat losses along zone i = f, d, c
$h_{i,rad}$	radiative losses along zone i = f, d, c
f_R	form factor for the smoldering surface
M	moisture, dry basis
$\dot{m}_f''$	mass consumption rate of virgin fuel
$\dot{m}_d''$	mass consumption rate of dry fuel
$\dot{m}_c''$	mass consumption rate of char
$\dot{m}_a''$	mass generation rate of ash
$\dot{m}_w''$	mass flow rate of water vapor
$\dot{m}_v''$	mass flow rate of volatiles
Q_{co}	heat of char oxidation
Q_p	heat of pyrolysis
Q_w	heat of vaporization of water
$\dot{q}_w''$	heat flux to preheat and vaporize water
$\dot{q}_v''$	heat flux to pyrolyze dry fuel
$\dot{q}_s''$	heat flux at smoldering front
$\dot{q}_{conv}''$	heat flux lost by convection
$\dot{q}_{rad}''$	heat flux by radiation
T	temperature
T_b	vaporization temperature
T_p	pyrolysis temperature
T_s	smoldering temperature

$T_{a,i}$	average temperatures at zone i = f, d, c
$T_{max,i}$	maximum temperature in zone i
T_0	initial temperature
T_∞	ambient temperature
U	smoldering rate
x_d	drying front position
x_s	smoldering front position
$Y_{O_2,\infty}$	ambient mass fraction of oxygen
$Y_{O_2,s}$	mass fraction of oxygen at smoldering surface

Greek symbols

α_i	effective heat diffusivity
β	O/F stoichiometric mass ratio
ε_s	emissivity of the smoldering surface
ε_i	emissivities of the zone surface i = f, d, c
ϕ_i	porosity of zone i = f, d, c
γ_i	effective convection coefficient around zone i = f, d, c
$\lambda_{s,i}$	solid thermal conductivity in zone i = f, d, c
$\lambda_{g,i}$	gas phase thermal conductivity in zone i = f, d, c
λ_i^*	effective heat conductivity in zone i = f, d, c
ρ_i	density of substance i = f, d, c, a
$\bar{\rho}_i$	average density of zone i = f, d, c
σ	Stefan–Boltzmann constant ($= 5.67 \times 10^{-8}$ W m^{-2} K^{-4})

Subscripts

f	unburned fuel
d	dry fuel
c	char
a	ash
w	water vapor
v	volatiles

general, the available solutions for natural or forced smoldering problems are obtained by numerical integration of systems of differential equations or by activation energy asymptotics.

An experimental investigation of smoldering in biomass was made by Carvalho et al. [19] in a laboratory facility (forced smoldering) and in prescribed forest burns (natural smoldering). They reported burn rates varying from 0.09 to 0.4 mm/min and pointed out that daytime rates were up to five times larger than nighttime rates due to higher ambient temperatures, higher wind speeds, and lower relative humidity. Carvalho [20] performed additional experiments

on smoldering of logs under controlled conditions in a specially built oven, using oven- and air-dried logs. Three different airflow rates, oven temperatures, and range diameters (10–32.5 cm) were tested. The average burn rate was 0.4–0.9 mm/min, with maximum temperatures 625–920 K, measured by thermocouples located in different positions inside the logs. Nevertheless only one test was performed for each condition and large cracks were formed along some logs. More extensive experiments are required to ensure sample independence. Additional observations by Carvalho [20] and Rabelo et al. [21] on natural smoldering of logs after prescribed burns have indi-

cated smolder rates varying from 0.1 to 0.4 mm/min and drying–pyrolysis thickness of a few centimeters ($\sim$ 10 cm). These logs were from different wood species with various moisture contents (11–47% dry basis) and diameters (17–68 cm).

Emissions from biomass smoldering were measured [1,2,22] and a large number of components, such as CO_2, CO, CH_4, C_2H_4, C_2H_2, C_3H_6, aldehydes, formic and acetic acids, alcohols, nitrogen, and sulfur compounds, were identified. However, the main products are CO and CO_2, at about 13 and 80 molar %, respectively, for several biomass species.

Moussa [3,4] described the reaction zone in a cellulosic material as a char oxidation region with high temperatures followed by a evaporation–pyrolysis region (350–700 K), where char, tar, and volatiles are formed by fuel degradation. The thickness of the reaction zone was found to be approximately equal to the sample diameter. Many factors, such as reaction rate, heat and mass transfer, and oxygen diffusion in the boundary layer, influence the processes occurring in the reaction zone. Smoldering logs present some different characteristics compared with other charring materials, such as cigarettes and cellulose cylinders. They have lower porosity than cigarettes or cotton and are characterized by formation of cracks in the char zone, ash deposition on soil, and complete escape of volatiles through the smoldering end, as longitudinal permeability is much higher (10^2–10^4) than radial permeability [23], assuming there is no preferential path along any holes inside the log.

The objective of this work is to present a comprehensive mathematical model to describe the natural smoldering of logs, assuming the steady one-dimensional propagation of infinitesimally thin fronts of drying, pyrolysis, and char oxidation in a horizontal semi-infinite log. The burn rates, distribution profiles of temperature, and drying–pyrolysis–smolder distances are obtained for logs with and without circumferential heat losses. A solution for a single drying–pyrolysis front is also presented. Effects

of variations of several parameters, such as pyrolysis temperature, heat of char oxidation, heat of pyrolysis, fuel density, fuel density, char density, moisture content, and log diameter, are evaluated.

2. Mathematical model

A schematic view of a circular cross section of a semi-infinite smoldering log is shown in Fig. 1. The log is divided into four regions: (1) the moist or unburned fuel zone, located at $x < x_d$; (2) the dry fuel zone, located at $x_d < x < 0$; (3) the char zone, located at $0 < x < x_s$; and (4) the ash zone, located at $x > x_s$. These regions are separated by three infinitesimally thin fronts: (1) a drying front, located at $x = x_d$, which is determined by the vaporization temperature of water, T_b ($\sim$ 373 K); (2) a pyrolysis front, located at $x = 0$, which is determined by the pyrolysis temperature of wood, T_P (> 500 K); and (3) a char oxidation front, located at $x = x_s$, which is determined by a smoldering temperature, T_s (> 650 K). It is considered a steady-state problem with all fronts moving at the same speed, i.e., the smoldering rate U.

The choice of fixed front temperatures corresponds to the assumption of infinite activation energies of drying, pyrolysis, and char oxidation in Arrhenius-type kinetics. It should be noted that parameters of char oxidation kinetics present large uncertainties and are measured for specific chars with given porosity and surface area [24]. In addition, wood can contain several inorganic components, inclusions, and resins which can significantly affect the char oxidation rates. The fast chemistry approach is useful to estimate global parameters such us smolder rates and drying/pyrolysis/smoldering distances, but does not allow accurate description of the density and temperature profiles inside the log.

It is assumed that all water contained in the wood is released at the drying front. At the pyrolysis front, the volatiles are released by producing char mixed
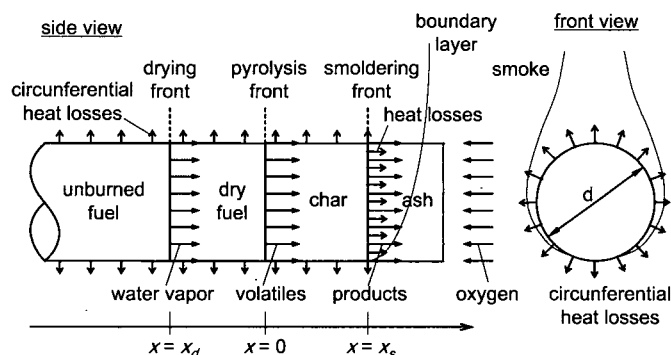

Fig. 1. One-dimensional smoldering of a log.

with ash, and at the smoldering front, char is oxidized by the ambient oxygen, forming CO and CO_2, and leaving ash on soil. All gases released in the fronts flow away from the moist material. A natural convection boundary layer adjacent to the smoldering front and that is not affected by the presence of ash (in practice, ash is carried away by wind or deposited on soil) is also assumed. In addition, heat is lost to the ambient by convection and by radiation around the log circumferential area and from the smoldering end.

Additional assumptions for the present analysis include: (1) one-dimensional burning; (2) natural thermal–viscous boundary layer adjacent to the smoldering front; (3) steady-state problem; (4) semi-infinite log; (5) exit of volatiles through the smoldering surface without reacting with the char; (6) ash layer thickness that does not affect flow; (7) pure carbon char; (8) neglect of soil radiation effects; (9) no effects of crack formation; (10) no holes or inclusions inside the log; and (11) thermal equilibrium between the gas and solid phases.

2.1. Energy equations

Using a moving reference frame following the reaction fronts, the balance energy equations can be written as

$$\dot{m}''_f c_{p,f} \frac{dT}{dx} = \lambda^*_f \frac{d^2T}{dx^2} - \frac{4h^*_f}{d}(T - T_0) \qquad (1)$$

for the moist wood zone, $-\infty < x < x_d$,

$$\left(\dot{m}''_d c_{p,d} + \dot{m}''_w c_{p,w}\right)\frac{dT}{dx} = \lambda^*_d \frac{d^2T}{dx^2} - \frac{4h^*_d}{d}(T - T_0) \qquad (2)$$

for the dry wood zone, $x_d < x < 0$, and

$$\left(\dot{m}''_c c_{p,c} + \dot{m}''_a c_{p,a} + \dot{m}''_v c_{p,v} + \dot{m}''_w c_{p,w}\right)\frac{dT}{dx}$$
$$= \lambda^*_c \frac{d^2T}{dx^2} - \frac{4h^*_c}{d}(T - T_0) \qquad (3)$$

for the char zone, $0 < x < x_s$. The subscripts f, d, c, a, w, and v denote unburned fuel, dry fuel, char, ash, water vapor and volatiles, respectively. T is the temperature at any position; T_0 is the log initial temperature; d is the log diameter; x_d is the drying front position; x_s is the smoldering front position; $\dot{m}''_f$ is mass consumption rate of virgin fuel; $\dot{m}''_d$ is the mass consumption rate of dry fuel; $\dot{m}''_c$ is the mass consumption rate of char; $\dot{m}''_a$ is the mass production rate of ash; $\dot{m}''_w$ is the mass flow rate of water vapor; $\dot{m}''_v$ is the mass flow rate of volatiles; λ^*_i is the effective heat conductivity in zone $i =$ f, d, c; h^*_i is the heat convection coefficient along zone $i =$ f, d, c, and $c_{p,i}$ is the specific heat of substance $i =$ f, d, c, a, w, v.

The term on the left-hand side in the energy balance equations for each zone corresponds to the energy transport by convection, the first term on the right-hand side corresponds to the energy transport by conduction and internal radiation, and the second term on the right-hand side corresponds to heat losses to the ambient by radiation and convection around the log circumference.

The mass fluxes are given by $\dot{m}''_f = \rho_f U$, $\dot{m}''_d = \rho_d U$, $\dot{m}''_c = \rho_c U$, $\dot{m}''_a = \rho_a U$, $\dot{m}''_w = (\rho_f - \rho_d)U$, and $\dot{m}''_v = (\rho_d - \rho_c - \rho_a)U$, where ρ_i is the density of substance $i =$ f, d, c, a.

The unburned fuel density and the dry fuel density are related by the moisture content M, on a dry basis:

$$\rho_d = \frac{\rho_f}{1 + M}. \qquad (4)$$

The specific heat of wood is calculated from [25]

$$c_{p,f} = \frac{c_{p,d} + M c_{p,l}}{1 + M} + A_c \ \text{J/(kg K)}, \qquad (5a)$$

$$c_{p,d} = 103.1 + 3.867 T_0 \ \text{J/(kg K)}, \qquad (5b)$$

where $A_c = M(-6.191 + 0.0236 T_0 - 0.0133 M)$ is an adjustment factor that accounts for the additional energy in the wood–water bond. It is valid below the fiber saturation point, $M \sim 0.3$, for $280 \ \text{K} < T_0 < 420 \ \text{K}$.

Porosity of wood can be related to moisture and density by the following equation, valid for $M < 0.3$ [26,27]:

$$\phi_f = 1 - \frac{\rho_f}{1500 - 1.35 \rho_f M}. \qquad (6)$$

And the char porosity can be obtained from

$$\phi_c = 1 - \frac{\rho_c}{\rho_{carbon}}, \qquad (7)$$

where $\rho_{carbon} = 1957 \ \text{kg/m}^3$. These equations indicate that low-density wood has a larger porosity than high-density wood, and that low moisture content increases the porosity.

It is assumed in the present model that the gas and solid phases are in thermal equilibrium. The effective heat conductivity, λ^*_i, includes a conduction term, $\lambda_{i,c}$, and an internal radiation term, $\lambda_{i,r}$:

$$\lambda^*_i = \lambda_{i,c} + \lambda_{i,r}, \quad i =$$ f, d, c, $\qquad (8)$

$$\lambda_{i,c} = (1 - \phi_i)\lambda_{s,i} + \phi_i \lambda_{g,i}, \qquad (9)$$

$$\lambda_{i,r} = \frac{16}{3}\sigma d_{p,i} T^3_{max,i}. \qquad (10)$$

Here $d_{p,i}$ is the average pore diameter in zone i, $\lambda_{s,i}$ is the solid thermal conductivity in zone i, $\lambda_{g,i}$ is the gas-phase thermal conductivity in zone i, $T_{max,i}$ is the maximum temperature in zone i, and σ is the Stefan–Boltzmann constant. This form of radiation conductivity has been used by Leach et al. [18].

The importance of the conduction and radiation terms varies along the log. Generally, in the char zone the radiation term is larger than the conduction term, whereas in the virgin and dry fuel zones, the conduction terms are much larger than the radiation term.

The moist wood thermal conductivity, for $M < 0.4$ and conduction parallel to the grain, in terms of moisture content, initial temperature, and oven dry density, is given by

$$\lambda_{s.f.0} = 0.0418\left(0.568 + (4.78 + 9.7M)\rho_d/1000\right)$$

$$\text{W}/(\text{m K}),\tag{11}$$

$$\lambda_{s,f} = 1.8(T_0/298)\lambda_{s,f,0} \text{ W}/(\text{m K}),\tag{12a}$$

and the dry wood conductivity is

$$\lambda_{s,d} = 0.0427(T_0/298) \text{ W}/(\text{m K}).\tag{12b}$$

These expressions are based on the results of Kollman, MacLean and Akita as reported by Kanury and Blackshear [26]. The correction factor 1.8 was included for longitudinal thermal conduction.

The effective heat transfer coefficient along zone i, h_i^*, assumed as a constant, is given by

$$h_i^* = h_{i,cv} + h_{i,r}, \quad i = \text{f, d, c},\tag{13}$$

$$h_{i,r} \cong \varepsilon_i \sigma (T_{a,i} + T_\infty)(T_{a,i}^2 + T_\infty^2),\tag{14}$$

where $h_{i,cv}$ corresponds to convective heat losses, $h_{i,r}$ corresponds to radiative losses, ε_i are emissivities of the i zone surface, T_∞ is the ambient temperature, and $T_{a,i}$, $i = $ f, d, c, are average temperatures of the unburned fuel, dry fuel, and char zones, respectively, and are given by $T_{a,f} = 0.5(T_\infty + T_b)$, $T_{a,d} = 0.5(T_b + T_P)$, and $T_{a,c} = 0.5(T_s + T_P)$.

The convective heat transfer coefficients are obtained from the literature in terms of the Grashof, Prandtl, and Nusselt numbers for natural convection around horizontal cylinders [28].

2.2. Boundary and coupling conditions

The following boundary and coupling conditions are used in the problem:

$$T(-\infty) = T_0, \qquad T(0) = T_p,\tag{15a}$$

$$T(x_d) = T_b, \qquad T(x_s) = T_s,\tag{15b}$$

$$\lambda_f^* T_x(x_d^-) = \lambda_d^* T_x(x_d^+) + \dot{q}_w'',\tag{15c}$$

$$\lambda_d^* T_x(0^-) = \lambda_c^* T_x(0^+) + \dot{q}_v'',\tag{15d}$$

$$\lambda_c^* T_x(x_s^-) = \dot{q}_s'',\tag{15e}$$

$$\dot{q}_w'' = \dot{m}_w''\left(Q_w - c_{p,l}(T_b - T_0)\right),\tag{15f}$$

$$\dot{q}_v'' = \dot{m}_v'' Q_P,\tag{15g}$$

$$\dot{q}_s'' = \dot{m}_c'' Q_{co} - \dot{q}_{conv}'' - \dot{q}_{rad}'',\tag{15h}$$

where Q_{co} is the heat of char oxidation, Q_P is the heat of pyrolysis, Q_w is heat of vaporization of water, $\dot{q}_w''$ is heat flux to preheat and vaporize water, $\dot{q}_v''$ is heat flux to pyrolyze dry fuel, $\dot{q}_s''$ is heat flux at the smoldering front, $\dot{q}_{conv}''$ is heat flux lost by convection, and $\dot{q}_{rad}''$ is heat flux lost by radiation. The SI units of Q_i and $\dot{q}_i''$ are J/kg and W/m², respectively.

At the smoldering front, heat can be lost by either convection or radiation. The radiation loss is given by

$$\dot{q}_{rad}'' = \varepsilon_s f_R \sigma \left(T_s^4 - T_\infty^4\right),\tag{16}$$

where ε_s is the emissivity of the smoldering surface and f_R is the form factor (nondimensional) for the smoldering surface. The form factor for a real log should be less than unity as a concave surface is often formed at the smoldering end (approximately conical with a vertex angle of about 60°). For a right circular cone, the form factor is $f_R = 1/(1 + h^2/r^2)^{1/2}$, where h is the height and r is the base radius. Therefore, for a 60° cone, $f_R = 0.5$. It should be noted that for a cigarette, the form factor should be larger than unity, because the radiating area is convex. Fig. 2 shows a common smoldering log cavity and typical smoldering in crossing logs. These crossings usually form burning fronts at 60° to the soil, created by the shear stress in the logs produced by their own weight, with each log section heating up the other log sections and low heat dissipation maintaining the smoldering process.

Heat transfer by convection at the smoldering front is given by

$$\dot{q}_{conv}'' = h_s(T_s - T_0),\tag{17}$$

with

$$h_s = h_0 \frac{\ln(1 + B_s)}{B_s},\tag{18}$$

where h_s is the convection heat transfer coefficient with blowing at the smoldering front, h_0 is the convection heat transfer coefficient without blowing, and B_s is the smoldering transfer number, which is used as a blowing factor for correction of the convection heat transfer coefficient. The transfer number represents the ratio of the driving force for smoldering to the resistance to smoldering. Values of heat transfer coefficients for natural convection along a vertical wall [25] were used by considering a square wall having the same area of the log circular cross section.

A mass balance of oxygen at the smoldering surface yields an expression for the smolder transfer number,

$$B_s = \frac{Y_{O_2,\infty} - Y_{O_2,s}}{\beta \rho_c/\rho_f + Y_{O_2,s}},\tag{19}$$

where β is the O/F stoichiometric mass ratio, $Y_{O_2,\infty}$ is the ambient mass fraction of oxygen, and $Y_{O_2,s}$ is
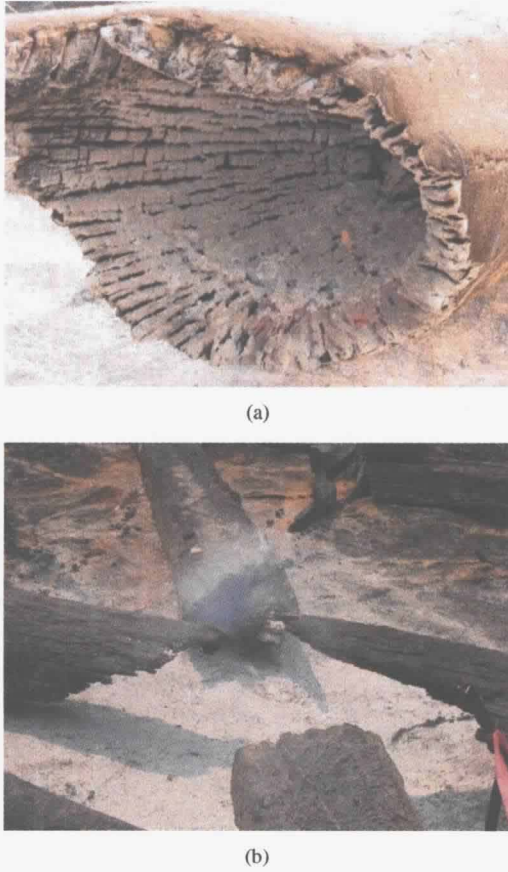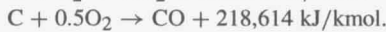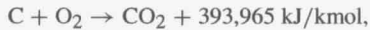
(a)

(b)

Fig. 2. Smoldering logs: (a) cavity in a smoldering log; (b) smoldering in crossing logs.

the mass fraction of oxygen at the smoldering surface. Because fast char oxidation kinetics was assumed, the smolder process is diffusion controlled, i.e., $Y_{O_2,s} = 0$.

The primary reactions describing char oxidation are

$$C + O_2 \rightarrow CO_2 + 393{,}965 \text{ kJ/kmol,}$$
$$C + 0.5O_2 \rightarrow CO + 218{,}614 \text{ kJ/kmol.}$$

These equations can be combined to yield the global reaction

$$C + aO_2 \rightarrow (2 - 2a)CO$$
$$+ (2a - 1)CO_2 + Q_{co}, \quad (20)$$
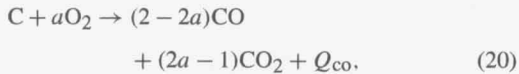
$$Q_{co} = 3.6 + 29.2a \text{ MJ/kg,} \quad (21)$$

where a is the stoichiometric coefficient of O_2 ($1/2 < a < 1$). An a of 15/16 gives a O/F stoichiometric mass ratio β of 2.5, with $Q_{co} = 31$ MJ/kg. This choice of a gives a fraction of 14% CO and 86% CO_2, in volume, respectively. Secondary surface reactions and gas-phase reactions are neglected.

2.3. Solution of the governing equations

The previous energy equations can be simplified, taking the form:

$$\alpha_i \frac{d^2 T}{dx^2} - U \frac{dT}{dx} - \gamma_i (T - T_0) = 0, \quad i = \text{f, d, c,} \quad (22)$$

with

$$\alpha_i = \lambda_i^* / (\bar{\rho}_i \bar{c}_{p,i}), \quad (23)$$
$$\gamma_i = 4h_i^* / (\bar{\rho}_i \bar{c}_{p,i} d), \quad (24)$$

where α_i is the effective heat diffusivity and γ_i is the effective convection coefficient along zone $i = f$, d, c. The average heat capacities, $\bar{\rho}_i \bar{c}_{p,i}$, are given by

$$\bar{\rho}_f \bar{c}_{p,f} = \rho_f c_{p,f}, \quad (25)$$
$$\bar{\rho}_d \bar{c}_{p,d} = \rho_d c_{p,d} + (\rho_f - \rho_d) c_{p,w}, \quad (26)$$
$$\bar{\rho}_c \bar{c}_{p,c} = \rho_c c_{p,c} + \rho_a c_{p,a} + (\rho_f - \rho_d) c_{p,w}$$
$$+ (\rho_d - \rho_c - \rho_a) c_{p,v}. \quad (27)$$

Solution of the problem requires the calculation of nine variables: six integration constants, the drying front position, x_d, the smoldering front position, x_s, and the smoldering rate, U. There are nine boundary and coupling conditions for the three zones: T_0, T_b, T_b, T_P, T_P, T_s, $\dot{q}''(x_d)$, $\dot{q}''(0)$, and $\dot{q}''(x_s)$.

2.4. Problem with no circumferential heat losses

Initially, integration of the governing equations with no circumferential heat losses, i.e., with $\gamma_i = 0$, is considered. By use of the above boundary and coupling conditions, the expressions for the temperature profiles are obtained as follows:

$$T = T_0 + (T_b - T_0)e^{U(x - x_d)/\alpha_f}, \quad -\infty < x < x_d, \quad (28a)$$

$$T = T_P - (T_P - T_b)\frac{1 - e^{Ux/\alpha_d}}{1 - e^{Ux_d/\alpha_d}}, \quad x_d < x < 0, \quad (28b)$$

$$T = T_P + (T_s - T_P)\frac{1 - e^{Ux/\alpha_c}}{1 - e^{Ux_s/\alpha_c}}, \quad 0 < x < x_s. \quad (28c)$$

The drying and smoldering front positions are given, respectively, by

$$x_d = -\frac{\alpha_d}{U} \ln\left(1 + \bar{\rho}_d \bar{c}_{p,d}(T_P - T_b)\right)$$
$$\times \left(\rho_f c_{p,f}(T_b - T_0)\right.$$
$$\left. - (\rho_f - \rho_d)\left(Q_w - c_{p,l}(T_b - T_0)\right)\right)^{-1}\right) \quad (29)$$

and

$$x_s = -\frac{\alpha_c}{U} \ln\left(1 - \bar{\rho}_c \bar{c}_{p,c}(T_s - T_P)\right.$$

$$\times \left(\rho_c Q_{co} - (h_s(T_s - T_\infty)\right.$$

$$\left. + \varepsilon_s f_R \sigma (T_s^4 - T_\infty^4))/U\right)^{-1}). \qquad (30)$$

and the burning rate is obtained from

$$U = \frac{h_s(T_s - T_\infty) + \varepsilon_s f_R \sigma (T_s^4 - T_\infty^4)}{\rho_c Q_{co} - E_f - E_d - E_c - E_a - E_w - E_v}, \qquad (31)$$

with

$$E_f = \rho_f c_{p,f}(T_b - T_0), \qquad (32a)$$

$$E_d = \rho_d c_{p,d}(T_P - T_b), \qquad (32b)$$

$$E_a = \rho_a c_{p,a}(T_s - T_P), \qquad (32c)$$

$$E_w = (\rho_f - \rho_d)$$

$$\times \left[c_{p,l}(T_b - T_0) + c_{p,w}(T_s - T_b) - Q_w\right], \qquad (32d)$$

$$E_v = (\rho_d - \rho_c - \rho_a)[c_{p,v}(T_s - T_P) - Q_P], \qquad (32e)$$

where E_f is the energy required to heat fuel to boiling temperature; E_d is the energy required to heat the dry fuel to pyrolysis temperature; E_c is the energy required to heat the char to smoldering temperature; E_a is the energy to heat ash to smoldering temperature; E_w is the energy required to vaporize water; and E_v is the energy required to pyrolyze and heat volatiles. The SI units of $E_{i=f,d,c,a,w,v}$ are J/m^3.

Eq. (31) can be misleading since one may think that increasing heat losses cause higher smolder rates. Nevertheless, Eq. (31) shows that the net energy flux from the smoldering reaction, $U(\rho_c Q_{co} - \sum E_i)$, has to be equal to the rates of radiation and convection heat losses, to allow the steady propagation of the reaction fronts. High smolder temperatures, resulting from fast smolder reactions, produce high smolder rates and also, correspondingly, high heat losses. An expression similar to Eq. (31) can be easily derived from Gugan's [6] results for maximum temperatures of smoldering cigarettes. Drysdale [29] used the simple relation $U = \dot{q}''/\rho \Delta h$ to estimate smolder rates of several charring materials, where $\dot{q}''$ is the net energy flux across the plane of inception, which was taken as the conduction heat flux at $x = 0$, roughly approximated by $k(T_s - T_0)/x_s$. This net energy flux must be proportional to the heat release rate minus the heat loss rate from the char zone. Moussa et al. [4] obtained an approximate analytical expression relating the interface temperature at the end of the pyrolysis zone (equivalent to the plane of inception) to the smolder rates. The heat flux at this plane was taken as half of the heat release rate minus the heat loss rate from the char oxidation zone. Because the heat release rate depends directly on the smolder rate, the expressions obtained by Drysdale and Moussa et al. for the smolder rate can be put in a form similar to Eq. (31).

Torero et al. [30] have obtained expressions for the natural smolder rates of polyurethane foam, dependent on oxidizer velocities and ignition heat fluxes. They considered an upward propagation of the smolder front and used the Darcy law coupled to the buoyancy force to calculate the oxidizer velocity.

When the maximum temperature T_s is known or measured, the smolder rate U can be easily calculated from Eq. (31), and vice versa. Alternatively, the heat of char oxidation Q_{co} can be found from the last expression if T_s and U are measured. It can be seen that $U > 0$ if $\rho_c Q_{co} > \sum E_i$. Otherwise, if $\rho_c Q_{co} < \sum E_i$, external energy has to be added to sustain the smoldering process. Explicit expressions for influence coefficients, $e_\phi = (\phi/\psi)d\psi/d\phi$, of a given parameter $\phi = T_P, Q_{co}, Q_P, \rho_f, \rho_c, \rho_a, M$, etc., on a variable $\psi = U, x_d, x_s$, etc., can be easily obtained from Eq. (31).

An alternative expression for the burn rate can be obtained by using the oxygen transport equation at the diffusion boundary layer,

$$U = \frac{\rho_\infty D_\infty}{\rho_f \delta} \ln(1 + B_s), \qquad (33).$$

where δ is the diffusion layer thickness, ρ_∞ is the ambient density, and D_∞ is the oxygen diffusivity at ambient conditions. δ depends on smolder temperature and on gas properties, but cannot be accurately determined unless the complete three-dimensional gas-phase problem is solved.

2.5. Problem with circumferential heat losses

If circumferential heat losses are considered the following expressions for temperature profiles are obtained:

$$T = T_0 + (T_b - T_0)e^{\frac{U(1+\Delta_f)(x-x_d)}{2\alpha_f}},$$

$$-\infty < x < x_d, \qquad (34a)$$

$$T = T_0 + C_{1,d}e^{\frac{U(1+\Delta_d)x}{2\alpha_d}} + C_{2,d}e^{\frac{U(1-\Delta_d)x}{2\alpha_d}},$$

$$x_d < x < 0, \qquad (34b)$$

$$T = T_0 + C_{1,c}e^{\frac{U(1+\Delta_c)x}{2\alpha_c}} + C_{2,c}e^{\frac{U(1-\Delta_c)x}{2\alpha_c}},$$

$$0 < x < x_s. \qquad (34c)$$

Here

$$\Delta_i = \sqrt{1 + 4\frac{\alpha_i \gamma_i}{U^2}}, \quad i = f, d, c, \qquad (35)$$

$$C_{1,d} = \frac{(T_b - T_0) - (T_P - T_0)e^{\frac{U(1-\Delta_d)x_d}{2\alpha_d}}}{e^{\frac{U(1+\Delta_d)x_d}{2\alpha_d}} - e^{\frac{U(1-\Delta_d)x_d}{2\alpha_d}}}. \qquad (36a)$$

$$C_{2,\mathrm{d}} = -\frac{(T_\mathrm{b} - T_0) - (T_\mathrm{P} - T_0)e^{\frac{U(1+\Delta_\mathrm{d})x_\mathrm{d}}{2\alpha_\mathrm{d}}}}{e^{\frac{U(1+\Delta_\mathrm{d})x_\mathrm{d}}{2\alpha_\mathrm{d}}} - e^{\frac{U(1-\Delta_\mathrm{d})x_\mathrm{d}}{2\alpha_\mathrm{d}}}}, \qquad (36\mathrm{b})$$

$$C_{1,\mathrm{c}} = \frac{(T_\mathrm{s} - T_0) - (T_\mathrm{P} - T_0)e^{\frac{U(1-\Delta_\mathrm{c})x_\mathrm{s}}{2\alpha_\mathrm{c}}}}{e^{\frac{U(1+\Delta_\mathrm{c})x_\mathrm{s}}{2\alpha_\mathrm{c}}} - e^{\frac{U(1-\Delta_\mathrm{c})x_\mathrm{s}}{2\alpha_\mathrm{c}}}}, \qquad (36\mathrm{c})$$

$$C_{2,\mathrm{c}} = -\frac{(T_\mathrm{s} - T_0) - (T_\mathrm{P} - T_0)e^{\frac{U(1+\Delta_\mathrm{c})x_\mathrm{s}}{2\alpha_\mathrm{c}}}}{e^{\frac{U(1+\Delta_\mathrm{c})x_\mathrm{s}}{2\alpha_\mathrm{c}}} - e^{\frac{U(1-\Delta_\mathrm{c})x_\mathrm{s}}{2\alpha_\mathrm{c}}}}. \qquad (36\mathrm{d})$$

Matching the coupling conditions at $x = x_\mathrm{d}$, $x = x_\mathrm{s}$, and $x = 0$ gives, respectively,

$$\frac{\lambda_\mathrm{f}^*}{\alpha_\mathrm{f}}(T_\mathrm{b} - T_0)(1 + \Delta_\mathrm{f})$$
$$= \frac{\lambda_\mathrm{d}^*}{\alpha_\mathrm{d}}\left(C_{1,\mathrm{d}}(1 + \Delta_\mathrm{d})e^{\frac{U(1+\Delta_\mathrm{d})x_\mathrm{d}}{2\alpha_\mathrm{d}}}\right.$$
$$\left. + C_{2,\mathrm{d}}(1 - \Delta_\mathrm{d})e^{\frac{U(1-\Delta_\mathrm{d})x_\mathrm{d}}{2\alpha_\mathrm{d}}}\right) + 2\frac{\dot{q}_\mathrm{w}''}{U}, \qquad (37\mathrm{a})$$

$$\frac{\lambda_\mathrm{c}^*}{\alpha_\mathrm{c}}\left(C_{1,\mathrm{c}}(1 + \Delta_\mathrm{c})e^{\frac{U(1+\Delta_\mathrm{c})x_\mathrm{s}}{2\alpha_\mathrm{c}}}\right.$$
$$\left. + C_{2,\mathrm{c}}(1 - \Delta_\mathrm{c})e^{\frac{U(1-\Delta_\mathrm{c})x_\mathrm{s}}{2\alpha_\mathrm{c}}}\right) = 2\frac{\dot{q}_\mathrm{s}''}{U}, \qquad (37\mathrm{b})$$

$$\frac{\lambda_\mathrm{d}^*}{\alpha_\mathrm{d}}\left(C_{1,\mathrm{d}}(1 + \Delta_\mathrm{d}) + C_{2,\mathrm{d}}(1 - \Delta_\mathrm{d})\right)$$
$$= \frac{\lambda_\mathrm{c}^*}{\alpha_\mathrm{c}}\left(C_{1,\mathrm{c}}(1 + \Delta_\mathrm{c}) + C_{2,\mathrm{c}}(1 - \Delta_\mathrm{c})\right) + 2\frac{\dot{q}_\mathrm{v}''}{U}. \qquad (37\mathrm{c})$$

The solution of this system of nonlinear algebraic equations (37a)–(37c) yields the pyrolysis front position, the smoldering front position, and the burning rate. Substitution of their values into Eqs. (34)–(36) allows determination of the temperature profiles.

2.6. Solution for a single front of drying and pyrolysis

An expression for the smoldering rate and the smoldering–drying front distance can be obtained assuming that the drying front coincides with the pyrolysis front. In this case the smoldering front position is calculated from

$$x_\mathrm{s} = \frac{2\alpha_\mathrm{c}}{U(1 + \Delta_\mathrm{c})}$$
$$\times \ln\left[\frac{(\alpha_\mathrm{c}\dot{q}_\mathrm{s}''/U\lambda_\mathrm{c}^*) - 0.5(1 - \Delta_\mathrm{c})(T_\mathrm{s} - T_\infty)}{(T_* - T_\mathrm{P} + T_\infty)\Delta_\mathrm{c}}\right]. \qquad (38)$$

and the smoldering rate is obtained from

$$\frac{(T_*\Delta_\mathrm{c})^{1+\Delta_\mathrm{c}}}{|(T_* - T_\mathrm{P} + T_\infty)\Delta_\mathrm{c}|^{1-\Delta_\mathrm{c}}}$$
$$= \frac{|(\alpha_\mathrm{c}\dot{q}_\mathrm{s}''/U\lambda_\mathrm{c}^*) - 0.5(1 + \Delta_\mathrm{c})(T_\mathrm{s} - T_\infty)|^{1+\Delta_\mathrm{c}}}{|(\alpha_\mathrm{c}\dot{q}_\mathrm{s}''/U\lambda_\mathrm{c}^*) - 0.5(1 + \Delta_\mathrm{c})(T_\mathrm{s} - T_\infty)|^{1-\Delta_\mathrm{c}}}, \qquad (39)$$

where

$$T_* = \left(0.5(T_\mathrm{P} - T_\infty)A - B\right)/\bar{\rho}_\mathrm{c}\bar{c}_{\mathrm{p,c}}\Delta_\mathrm{c}, \qquad (40\mathrm{a})$$

$$A = \bar{\rho}_\mathrm{f}\bar{c}_{\mathrm{p,f}}(1 + \Delta_\mathrm{f}) - \bar{\rho}_\mathrm{c}\bar{c}_{\mathrm{p,c}}(1 + \Delta_\mathrm{c}), \qquad (40\mathrm{b})$$

$$B = (\rho_\mathrm{d} - \rho_\mathrm{c} - \rho_\mathrm{a})Q_\mathrm{P} + (\rho_\mathrm{f} - \rho_\mathrm{d})Q_\mathrm{w}. \qquad (40\mathrm{c})$$

3. Results and discussion

Attention is now focused on calculation of the properties of the smoldering process, considering circumferential heat losses and separate fronts of drying and pyrolysis. The characteristics of particular interest are burn rates, drying front position, smoldering front position, temperature profiles, and heat losses. In this context the purpose of this section is to discuss and to compare the effects of variations on moisture content, log diameter, heat of pyrolysis, pyrolysis temperature, and other parameters, by employing the reference data summarized in Table 1 and from Eqs. (4)–(14). Some experimental data are also compared with the theoretical results.

The effects of moisture content on burn rates, drying and smoldering front positions, and heat fluxes at the smoldering surface are illustrated in Fig. 3. In this case the char and the dry wood density were kept constant, while the virgin wood density changed with moisture content. The influence of log diameter on burn rates, positions, and heat fluxes is depicted in Fig. 4. The dependence of temperature profiles due to variations in moisture content, char density, and smoldering surface temperatures is displayed in Fig. 5. The influence coefficients of several parameters on burn rates and on drying and smolder front distances, for a fixed density ratio, $\rho_\mathrm{c}/\rho_\mathrm{d} = 0.2$, are shown in Fig. 6.

Table 1
Reference data used in the simulations

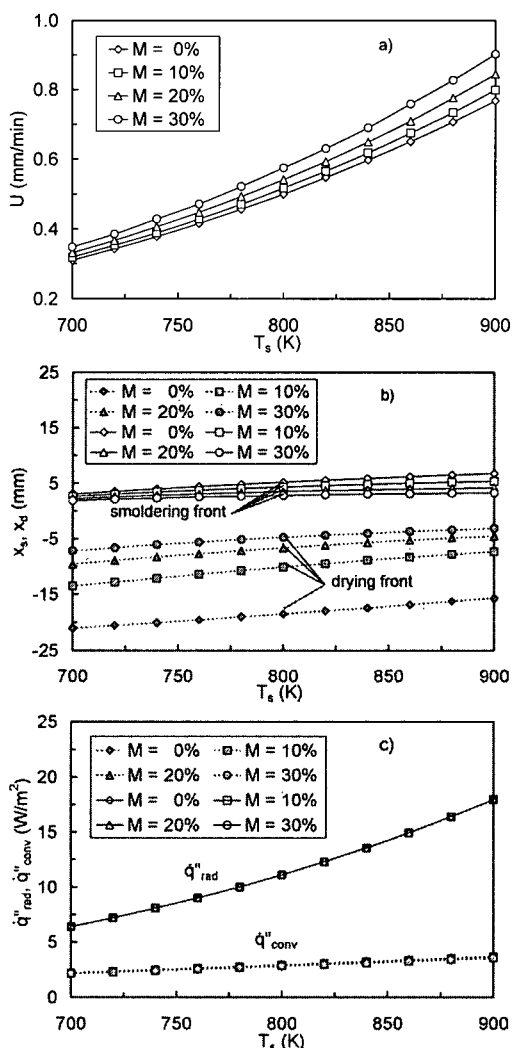| Property	Value	Units	Property	Value	Units
Q_P	−300	kJ/kg	T_b	373	K
Q_co	31	MJ/kg	T_p	600	K
Q_w	−2445	kJ/kg	T_0	315	K
$c_{\mathrm{p,c}}$	0.67	kJ/(kg K)	T_∞	315	K
$c_{\mathrm{p,v}}$	1.10	kJ/(kg K)	ε_f	0.75	—
$c_{\mathrm{p,w}}$	2.02	kJ/(kg K)	ε_d	0.75	—
$c_{\mathrm{p,l}}$	4.17	kJ/(kg K)	ε_c	0.98	—
λ_c	0.041	W/(m K)	$d_{\mathrm{p,f}}$	0.0001	m
λ_v	0.043	W/(m K)	$d_{\mathrm{p,d}}$	0.0001	m
λ_w	0.047	W/(m K)	$d_{\mathrm{p,c}}$	0.0003	m
ρ_f	432	kg/m^3	$Y_{\mathrm{O}_2,\infty}$	0.23	—
ρ_d	360	kg/m^3	$Y_{\mathrm{O}_2,\mathrm{s}}$	0	—
ρ_c	72	kg/m^3	M	20	%
ρ_a	10	kg/m^3	f_R	0.5	—
d	0.25	m			

Fig. 3. Effects of moisture content on smolder characteristics of logs: (a) burn rates; (b) pyrolysis front and smoldering front positions; (c) heat fluxes at the smoldering surface.
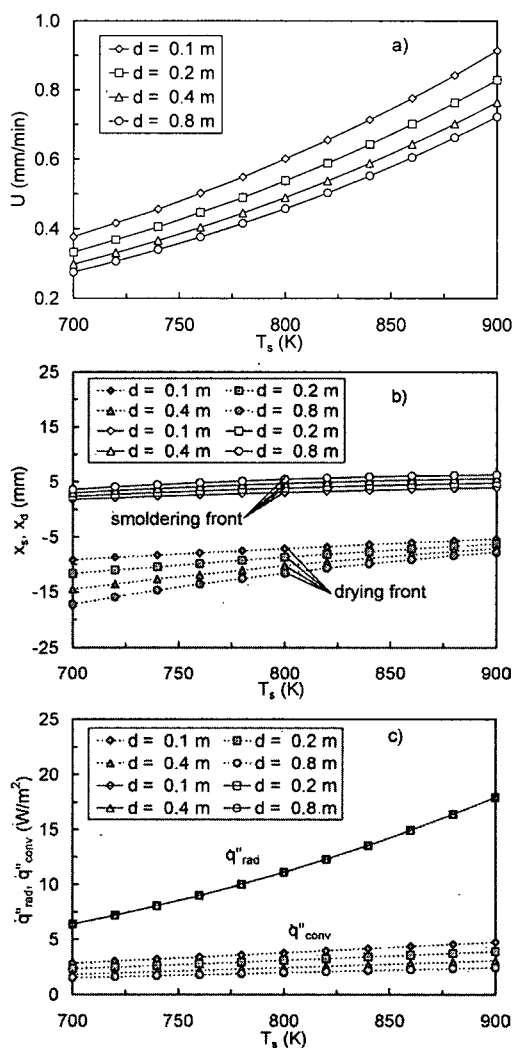
Fig. 4. Effects of diameter on smolder characteristics of logs: (a) burn rates; (b) pyrolysis front and smoldering front positions; (c) heat fluxes at the smoldering surface.

Burning rates varied from about 0.3 to 0.9 mm/min for the moisture contents and log diameters shown in Figs. 3 and 4, considering smolder temperatures between 700 and 900 K. Smolder front positions increase slightly as smolder temperatures increase, whereas drying front positions decrease significantly (in absolute value) as smolder temperatures increase. For a fixed burn rate, the smolder temperatures decreases as moisture content increases or log diameter decreases. Convective heat losses are smaller than radiation heat losses, for the assumed radiation form factor. Radiation heat losses can be six times larger than convective heat losses at 900 K. The convective heat losses per unit area increase as log diameter decreases, because the viscous–thermal boundary layer becomes thinner and, consequently, the temperature

gradient becomes larger. Moisture content had no effect on convective heat losses per unit area, because, in the present model, the convective heat transfer coefficients are not affected by the presence of water vapor. Moisture content and diameter do not affect radiative heat losses per unit area if a fixed smoldering temperature is considered. On the other hand, if smolder temperatures are affected by moisture, there will be changes in heat losses by radiation and by convection.

Fig. 4 shows that for fixed smolder temperatures, the drying front position gets farther as moisture content decreases or char density increases. Drying–pyrolysis distances vary from 7 to 30 mm and do not change significantly with smolder temperatures.
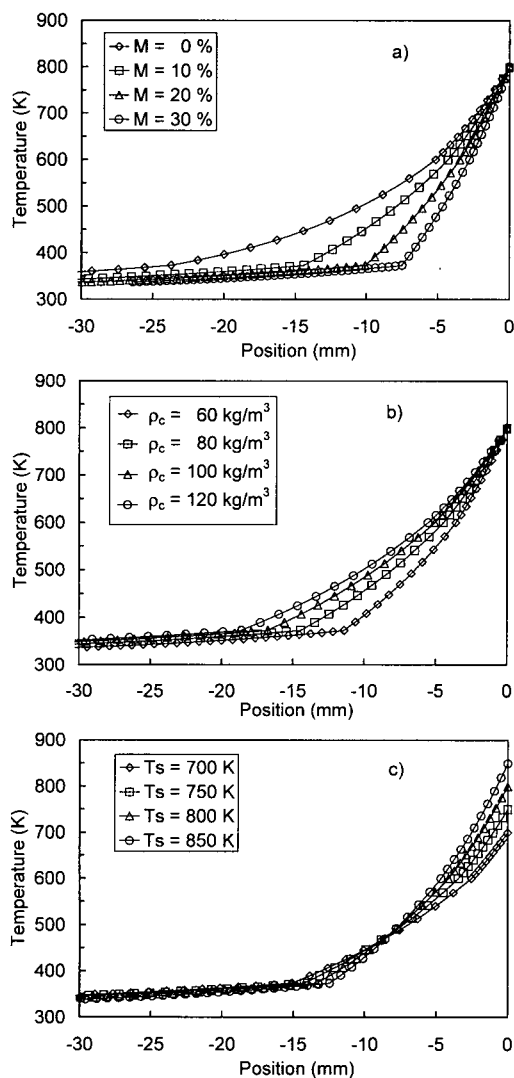
Fig. 5. Temperature profiles of smoldering logs: (a) effects of moisture content; (b) effects of char density; (c) effects of smoldering temperatures. Reference frame is now located on the smoldering front.

Experimental temperature profiles obtained from the date of Carvalho et al. [19] on three different logs are depicted in Fig. 7. The temperature profiles were calculated based on the average smolder rates of each log and the temperatures were measured by thermo-couples. T_i, located at several positions inside the logs. The smoldering surfaces were very rough and many cracks along the log surfaces were observed in the experiments, exposing several thermocouples (not those in Fig. 7). The logs were in contact with the oven bottom and the smoldering surfaces were not vertical. It is not clear in Fig. 7 which regions of the temperature profiles correspond to the pyrolysis or smoldering zones. However, in many curves,
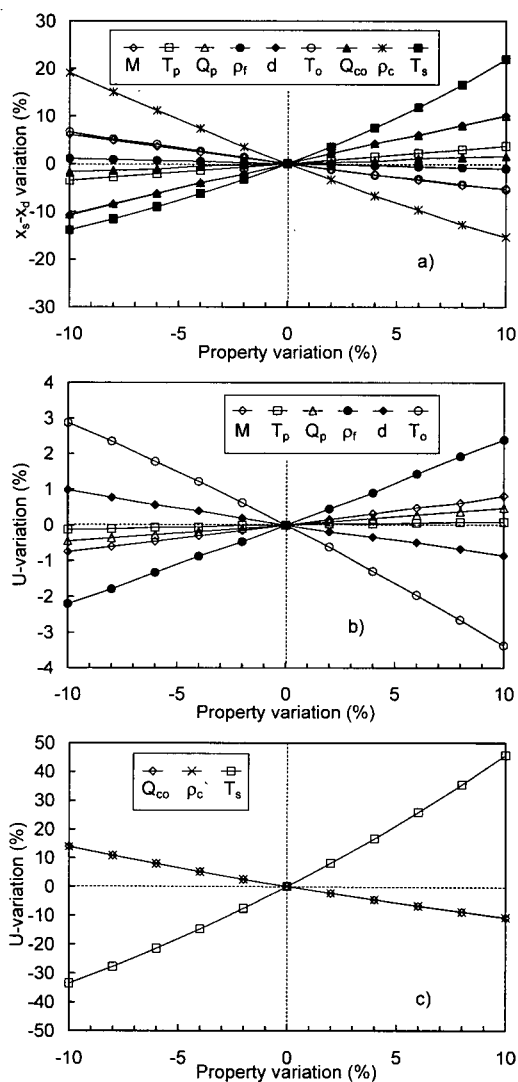
Fig. 6. Influence coefficients of several parameters on smoldering characteristics of logs. (a) Influence of M, T_P. Q_P, ρ_f, d, T_0, Q_{co}. ρ_c and T_s on drying–smolder front positions; (b) influence of M, T_P, Q_P, ρ_f, d, and T_0 on burn rates; (c) influence of Q_{co}, ρ_c. and T_s on burn rates. Reference $Q_{co} = 28$ MJ/kg.

the existence of two regions is observed with a linear increase in temperatures; these can be considered either as two pyrolysis zones, with different decomposition kinetics, or as a pyrolysis zone followed by a smoldering zone. The temperatures of thermocouples T1 and T2 of log 1 and T5 of log 3 stabilized at about 373 K along the drying zone, while the temperatures profiles of thermocouples T1 and T2 of log 5 had regions with constant intermediate temperatures, below 373 K.

In general, the experimental distances including the pyrolysis and smolder zones were larger than the

theoretical ones. This can be explained by the deep cracks formed on the smoldering front, convective heating from volatiles, and radiation from the char oxidation zone which increase the exposure time and keep the thermocouples heated before and after the reaction fronts have passed. Fast chemistry was also assumed in the theoretical model; however, usually, fast chemistry models do not yield correct temperature profiles, because reaction is considered to occur on an infinitesimally thin surface.

As shown in Fig. 5, the parameters with larger influence coefficients on burn rates are Q_{co}, ρ_c, and T_s, whereas T_s and ρ_c have greater influence on smolder–drying front distances. Interestingly, Q_{co} and ρ_c have the same influence on burn rates. Pyrolysis temperature and heat of pyrolysis have small effects on burn rates and on front positions. However, care should be taken when analyzing the influence coefficients, as each parameter is varied independently of the others. For example, moisture content can also affect smolder temperatures, but no relation between them was provided in the calculations. Also, char density is directly related to virgin wood density and an appropriate relationship could be used in the calculations.

Table 2 lists selected results of forced smoldering of logs obtained by Carvalho et al. [19]. The logs were from three species of *embaúba* trees from the
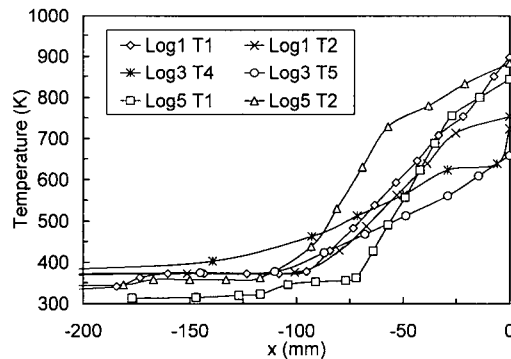

Fig. 7. Experimental temperature profiles of smoldering logs measured by thermocouples located in different sections of the logs. Data from Ref. [19]. Reference frame is located on the smoldering front.

Amazon forest: black, white, and *pata de anta*, belonging to genus *Cecropia*, family *Moraceae*. These species have an estimated average oven dry density of 360 kg/m^3 and average composition of $C = 43.46\%$, $H = 6.18\%$, $N = 0.44\%$. No clear correlation among airflow rates, oven temperatures, burning rates, maximum temperatures, and burning rates could be observed in the experiments due to sample variability.

Despite the inclusion of many details in the present model, it represents a first step in the description of the complex chemical and physical processes occurring during smoldering of logs. The model could be improved initially by considering finite rate kinetics for the drying and pyrolysis processes, diffusion of oxygen into the char pores with volumetric char oxidation, axisymmetric burning, and tar formation, deposition, and reaction inside the char pores.

4. Conclusions

A mathematical model was developed to estimate burn rates, temperature profiles, and positions of the drying, pyrolysis, and smolder fronts of a naturally smoldering log. A steady one-dimensional propagation of infinitesimally thin fronts in a semi-infinite log of circular section was assumed, considering heat conduction, convection, and radiation inside the porous matrix, and external radiation and convection around the log and inside the boundary layer adjacent to the smoldering end. A smolder transfer number was determined and a solution for the problem with a single drying–pyrolysis front was presented. The theoretical burning rates showed good agreement with available experimental data.

Acknowledgments

Table 2
Experimental data from Carvalho et al. [19] on smoldering logs

Log	Species	Drying	Average d (cm)	Air flow rate (L/min)	T_{oven} (K)	T_{max} (K)	U (mm/min)
1	Black	Air	14	85	298	900	0.67
2	White	Air	21	99	298	625	0.81
3	Pata de anta	Air	28	113	298	725	0.58
4	Pata de anta	Air	28	85	373	775	0.58
5	Black	Air	14	99	373	885	0.60
6	White	Air	21	113	373	760	0.52

References

[1] L.M. Mckenzie, W.M. Hao, G.N. Richards, D.E. Ward, Environ. Sci. Technol. 29 (1995) 2047–2054.

[2] R.J. Yokelson, R. Susott, D.E. Ward, J. Reardon, D.W.T. Griffith, J. Geophys. Res. 102 (D15) (1997) 18865–18877.

[3] N.A. Moussa, ScD thesis, Massachusets Institute of Technology, 1975.

[4] N.A. Moussa, T.Y. Toong, C.A. Garris, Proc. Combust. Inst. 16 (1976) 1447–1457.

[5] T.J. Ohllemiller, E. Rogers. A. Kurtz, J. Bellan, M. Summerfield, Two Year Summary Report to the National Bureau of Standards (Grant 4-906), Guggenhein Lab., Princeton University, Princeton, NJ, 1976.

[6] K. Gugan, Combust. Flame 10 (1966) 161–164.

[7] M. Summerfield, T.J. Ohlemiler. H.W. Sandusky, Combust. Flame 33 (1978) 263–279.

[8] M. Muramatsu, S. Umemura, T. Okada, Combust. Flame 36 (1979) 245–262.

[9] R.G. Gann, R.H. Harris Jr., J.F. Krasny, R. Levine, H.E. Mitler, T.J. Ohlemiller. NBS Tech. Note 1241, National Bureau of Standards, U.S. Dept. of Commerce, 1988.

[10] F.S. Costa, in: Proceedings of 2003 ASME: Summer Heat Transfer Conference. Las Vegas, NV, July 21–23, 2003, Paper HT2003-47311.

[11] S.C. Yi, E.U. Song, M.R. Hajaligol, J. Fire Sci. 19 (6) (2001) 429–448.

[12] K. Kailasanath, B.T. Zinn. in: Proc. Fluids Eng. Conf., 1981.

[13] A.M. Kanury, D.J. Holve, Trans. ASME 104 (1982) 338–343.

[14] M.J. Spearpoint, J.G. Quintiere, Combust. Flame 123 (2000) 308–324.

[15] J.L. Torero, A.C. Fernandez-Pello, Combust. Flame 106 (1996) 89–109.

[16] D.A. Schult, Matkowsky. V.A. Volpert, A.C. Fernandez-Pello, Combust. Flame 104 (1996) 1–26.

[17] J. Buckmaster, D. Lozinski, Combust. Flame 104 (1996) 300–310.

[18] S.V. Leach, G. Rein, J.L. Ellzey, O.A. Ezekoye, J.L. Torero, Combust. Flame 120 (2000) 346–358.

[19] E.R. Carvalho, C.A.G. Veras, J.A. Carvalho Jr., Biomass Bioenerg. 22 (2002) 283–294.

[20] E.R. Carvalho, Doctoral dissertation, UNESP, Brazil, 2003 (in Portuguese).

[21] E.R.C. Rabelo, C.A.G. Veras, J.A. Carvalho, E.C. Alvarado, D.V. Sandberg, J.C. Santos, Atmos. Env. 38 (2004) 203–211.

[22] R.J. Yokelson, D.W.T. Griffith, D.E. Ward, J. Geophys. Res. 101 (1996) 21067–21080.

[23] M. Gronli, M. Melaaen, in: Nordic Seminar on Biomass Gasification and Combustion, NTH, Trondheim, 30–31 August 1993.

[24] I.M. Bews, N. Hayhurst. S.M. Richardson, S. Taylor, Combust. Flame 124 (2001) 231–245.

[25] Wood Handbook—Wood as an Engineering Material, Gen. Tech. Rep. FPL-GTR-113, U.S. Dept. of Agriculture, Forest Service, Forest Products Laboratory, Madison, WI, 1999.

[26] A.M. Kanury, P.L. Blackshear, Combust. Sci. Technol. 2 (1970) 339–355.

[27] MacLean, USFPL Report No. R1448 (1944).

[28] Y. Jaluria, in: P.J. DiNenno, C.L. Beyler, R.L.P. Custer, W.D. Walton, J.M. Watts (Eds.), National Fire Protection Association, first ed., in: SFPE Handbook of Fire Protection Engineering, 1988, p. I.116.

[29] D. Drysdale, An Introduction to Fire Dynamics, second ed., Wiley. New York, 2002, pp. 276–277.

[30] J.L. Torero, A.C. Fernandez-Pello, M. Kitano. Fire Saf. J. 24 (1995) 35–52.